International Journal of Mass Spectrometry 309 (2012) 56–62

Contents lists available at SciVerse ScienceDirect

International Journal of Mass Spectrometry

journal homepage: www.elsevier.com/locate/ijms

Theoretical studies on structures and electronic spectra of linear HC_nN^+ (n = 2–14)

Yanxin Zhang, Jia Guo, Jinglai Zhang*

Institute of Environmental and Analytical Sciences, College of Chemistry and Chemical Engineering, Henan University, Kaifeng 475004, China

ARTICLE INFO

Article history:
Received 3 July 2011
Received in revised form 26 August 2011
Accepted 26 August 2011
Available online 3 September 2011

Keywords:
Linear HC_nN^+ (n = 2–14)
B3LYP
CASPT2
Incremental binding energy
Vertical excitation energy

ABSTRACT

With unrestricted B3LYP and CAM-B3LYP calculations, we have investigated the linear HC_nN^+ (n = 2–14) clusters focusing on the ground-state geometries, vibrational frequencies, rotational constants, dipole moments, energy differences (ΔE_n), and incremental binding energies (ΔE^I). The results indicate that the odd-numbered HC_nN^+ clusters have polyacetylene-like structures with significant single–triple bond length alternation, while the even-numbered analogues exhibit some sort of cumulenic character, with the former being more stable than the latter. The CASPT2/cc-pVTZ approach has been employed to estimate the vertical excitation energies for the dipole-allowed $(2, 3)^2\Pi \leftarrow X^2\Pi$ and dipole-forbidden $1^2\Phi \leftarrow X^2\Pi$ transitions in HC_nN^+ (n = 5–14) clusters. The predicted excitation energies of $2^2\Pi \leftarrow X^2\Pi$ transitions for HC_nN^+ (n = 5–13) clusters are 2.27, 2.33, 2.04, 2.02, 1.84, 1.76, 1.62, 1.58, and 1.49 eV, respectively, in good agreement with the available observed values (2.12, 2.17, 1.84, 1.89, 1.61, 1.66, 1.42, 1.49, and 1.27 eV). In addition, the higher electronic transitions of HC_nN^+ (n = 5–14) are also calculated. We expect that calculations for $3^2\Pi \leftarrow X^2\Pi$ transitions in odd-n clusters are able to contribute to further experimental and theoretical researches because of their relatively higher oscillator strengths. Finally, in the paper are discussed the possible dissociation channels and corresponding fragmentation energies of HC_nN^+ clusters.

1. Introduction

Carbonaceous molecules are reported to be widely present in interstellar [1] and circumstellar media. For recent several decades, these molecules have received considerable attention for their important roles in the formation of stars, protoplanetary disks, planetesimals, and in the study of the origin of life [2–5]. Most of these molecules are carbon chain clusters, including pure carbon clusters (C_2, C_3, etc.) [6] and substituted carbon clusters (C_8H, HC_8N, C_3S, etc.) [1,7–9]. Carbon clusters with general formula of C_nH_m ($m \leq n$) were also found to be existent in hydrocarbon flames and other soot-forming systems [10]. They were thought to be intermediates for many chemical reactions [6]. Spectroscopic characterization of carbon chains and their ions has been greatly motivated by a general interest in understanding the electronic structures and properties owing to their significance in astrophysics [11], combustion [12], cosmic chemistry, molecular electronics, and material science [13].

Among these carbon clusters, For one thing, cyanopolyacetylenes are quite interesting due to their unusual abundance and astrophysical importance in interstellar medium. For another, most of the polyatomic molecules in rich interstellar and circumstellar sources to date are carbon chains with alternating single and triple bonds [14,15]. As a result, cyanopolyacetylenes $HC_{2n+1}N$, with the existence of H–(C≡C)$_n$–C≡N, are well-studied molecules in the laboratory and in interstellar space. Chains up to $HC_{11}N$ have been detected in rich astronomical sources [16]. And later the linear $HC_{15}N$ and $HC_{17}N$ have also been detected in the laboratory by Fourier transform microwave spectroscopy [14]. We find the same case in cyanopolyacetylene cations, say, HC_5N^+ and HC_7N^+ [17–19] have received broad investigation. A detailed study of the rotationally resolved $A^2\Pi \leftarrow X^2\Pi$ 0_0^0 electronic transitions of the cyanodiacetylene (HC_5N^+) [17] and cyanotriacetylene (HC_7N^+) [19] cations was presented by Sinclair and his coworkers, who discussed the rotational constants of the two cations contemporaneously. Complementary to the work, Maier et al. made a report on the observed electronic spectra of cyanopolyacetylene cations $HC_{2n-1}N^+$ (n = 2–7) and $HC_{2n}N^+$ (n = 3–6) in the gas phase and neon matrices, which is a summary of the previous work in this system [20].

No doubt that numerous experimental data on the electronic spectra of HC_nN^+ are available [17–23], theoretically, however, the related calculations have been only limited to some separate molecules or the lowest electronic excitation states. As far as we know, Lee et al. optimized the geometries of the linear cyano-substituted polyacetylene cations, H–C_n–CN^+ (n = 4–11), using the UHF/4-31G level of theory and calculated the transition energies for the lowest $\pi \rightarrow \pi^*$ electronic excitations with the complete active

* Corresponding author. Tel.: +86 378 3881589; fax: +86 378 3881589.
E-mail address: zhangjinglai@henu.edu.cn (J. Zhang).

1387-3806/$ – see front matter © 2011 Elsevier B.V. All rights reserved.
doi:10.1016/j.ijms.2011.08.025

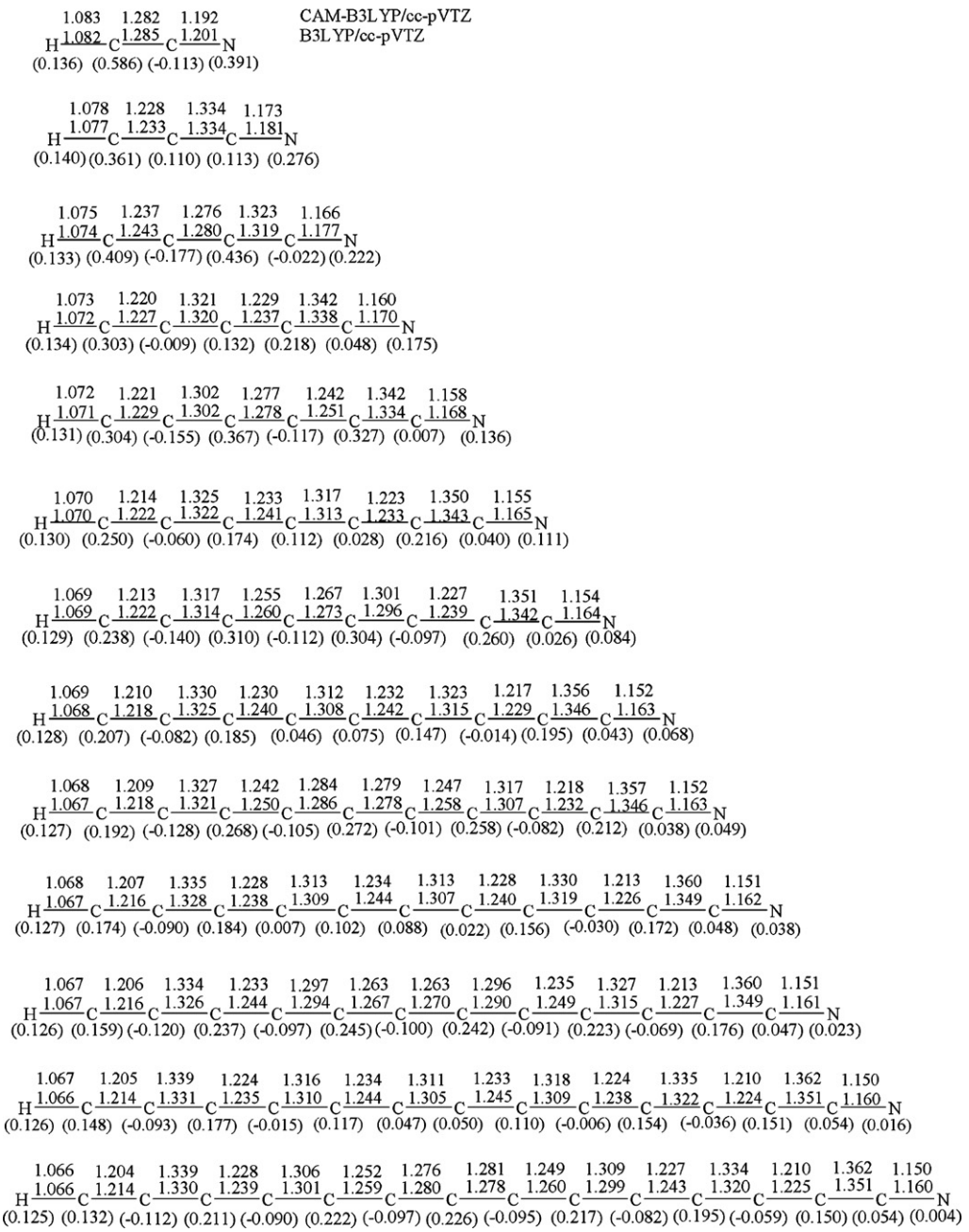

Fig. 1. B3LYP and CAM-B3LYP optimized bond lengths (in angstrom) and NBO charges (in parentheses) of the linear ground-state HC_nN^+ (n = 2–14) clusters.

space self-consistent field method (CASSCF) and the complete active space second-order perturbation theory method (CASPT2) [24]. Later, Cao et al. predicted the vertical transition energies for the strongest $2^2\Pi \leftarrow X^2\Pi$ transition and other higher $^2\Pi \leftarrow X^2\Pi$ transitions of HC_5N^+ by the multireference configuration interaction procedure (MRCI) [25].

To get a thorough understanding of the ground- and excited-states of HC_nN^+, therefore, a systematically theoretical study of structures and electronic spectra of the carbon clusters is necessary. Here, in the paper, we firstly investigated linear HC_nN^+ (n = 2–14) clusters on their ground-state bonding characters, vibrational frequencies, rotational constants, dipole moments, energy differences (ΔE_n), incremental binding energies (ΔE^1), and dissociation channels, illustrating the relative stability consistent with the regularity of odd/even alternation derived from previous studies of HC_nN clusters [26]. Then, the vertical excitation energies of HC_nN^+ (n = 5–14) were explored in detail by the highly accurate CASPT2 level of theory, which has been successfully applied to studies of $HC_{2n+1}H^+$ (n = 2–7) [27], $HC_{2n}H^+$ (n = 2–8) [28], $MgC_{2n}H$ (n = 1–5) [29], and the similar systems.

2. Computational details

The ground-state equilibrium geometries of linear HC_nN^+ (n = 2–14) clusters have been optimized by density functional (B3LYP [30–32] and CAM-B3LYP [33]) calculations along with the cc-pVTZ basis set. The nature of the optimized structures was evaluated by the frequency analyses and the odd/even regularity was explored by the energy calculations.

The vertical excitation energies (ΔE) for the dipole-allowed $(2, 3)^2\Pi \leftarrow X^2\Pi$ and dipole-forbidden $1^2\Phi \leftarrow X^2\Pi$ transitions of HC_nN^+ (n = 5–14) at the B3LYP/cc-pVTZ geometries have been

Table 1
The CASSCF active spaces of HC_nN^+ (n = 5–14) at the CASPT2 calculations.

Species	CASSCF active space	Electrons
HC_5N^+	(13,0,0,0/0,5,5,0)	11
HC_6N^+	(14,1,1,0/2,4,4,0)	11
HC_7N^+	(17,0,0,0/0,6,6,0)	15
HC_8N^+	(18,2,2,0/2,4,4,0)	11
HC_9N^+	(21,0,0,0/0,6,6,0)	19
$HC_{10}N^+$	(22,2,2,0/2,5,5,0)	15
$HC_{11}N^+$	(25,0,0,0/0,7,7,0)	23
$HC_{12}N^+$	(26,3,3,0/2,5,5,0)	15
$HC_{13}N^+$	(29,0,0,0/0,8,8,0)	27
$HC_{14}N^+$	(30,4,4,0/2,5,5,0)	15

investigated by CASPT2 [34] with the cc-pVTZ basis set. As shown in Table 1, the calculated CASSCF active space for even-n clusters consists of two σ valence orbitals and some low-energy π valence orbitals, while only some low-energy π valence orbitals are contained in odd-n clusters. Four numbers of the front group represent the number of inactive orbitals with symmetry labels a_1, b_1, b_2, and a_2, respectively, and figures of the latter stand for the number of active orbitals with similar symmetry.

In the CASPT2 calculation, the oscillator strengths (f) are calculated by the following formula:

$$f = \frac{2}{3}\Delta E\left|TM\right|^2 \quad (1)$$

where ΔE is the transition energy between the ground and excited states in atomic unit and TM refers to the transition dipole moment in atomic unit [35].

All calculations in the present work have been performed by the Gaussian 09 [36] and MOLPRO 2006 [37] program packages.

3. Results and discussion

3.1. Geometry configuration, vibrational frequencies, NBO charges, rotational constants, and dipole moments

3.1.1. Geometry configuration

The unrestricted B3LYP and CAM-B3LYP optimized bond lengths of linear HC_nN^+ (n = 2–14) clusters in their ground states are displayed in Fig. 1. Bond lengths predicted by the two methods are almost identical with the maximum deviation of 0.014 Å. When n is odd, the C–C bond lengths exhibit a significant polyacetylene-like character, which is a series of single–triple bond alternate pattern marked with a regular alternation of long (~1.305–1.351 Å) and short (~1.214–1.245 Å) bonds at B3LYP/cc-pVTZ theoretical level. C–C bond lengths of even-numbered clusters show the similar long/short alternation. But the trend weakens along from both ends to the center of the corresponding chains and the pattern gradually fades to exhibit some sort of cumulenic character. Fig. 2 depicts the bond lengths of linear $HC_{13}N^+$ and $HC_{14}N^+$ clusters versus i (i means the number from one bond to the other beginning with C–H bond), which is an illustration to the parity alternation in the HC_nN^+ (n = 2–14) clusters. Additionally, C–N bond lengths tend to decrease with the extension of carbon chains, which may imply higher and higher C–N bond energies.

3.1.2. Vibrational frequencies

In order to further analyze the nature of optimized structures, we calculated the vibrational frequencies and IR intensities of HC_nN^+ (n = 2–14) clusters at the B3LYP equilibrium geometries (see Table S1 in Supplementary Information). The lowest bending vibrational frequencies are 66, 205, 120, 104, 75, 61, 47, 40, 33, 28, 24, 21, and 18 cm^{-1}, respectively, and without imaginary frequency, indicating that carbon chains in Fig. 1 are stable structures on the potential energy surfaces (PES).

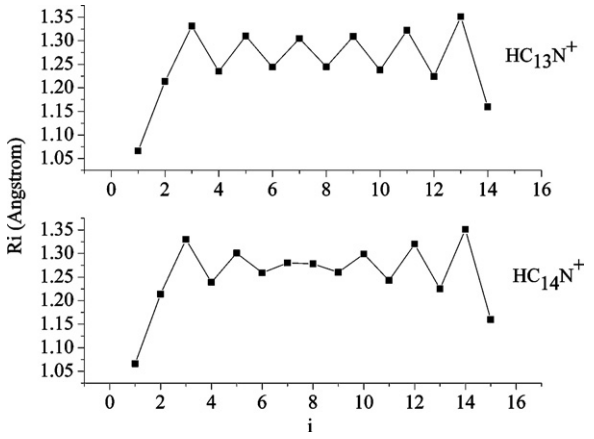

Fig. 2. Bond lengths (in angstrom) of all the bonds along the linear $HC_{13}N^+$ and $HC_{14}N^+$ chains at the B3LYP/cc-pVTZ level. "i" is numbered starting from one to the other beginning from C–H bond.

3.1.3. NBO charges

Also displayed in Fig. 1 are the NBO atomic charges (values in parentheses underneath the atoms) of the linear HC_nN^+ (n = 2–14) clusters. According to Fig. 1, positive charges located on the terminal H and N atoms decrease gradually as the carbon chains lengthen. For even-n clusters, the odd C atoms counting from H atom bear more positive charges and even C atoms more negative charges. While in terms of odd-n counterparts, still a large proportion of positive charges are distributed over the C atoms next to H besides the terminal H and N atoms. And charges on other C atoms tend to be more and more dispersed with a rise in n.

3.1.4. Rotational constants

Table 2 lists the calculated rotational constants of HC_nN^+ (n = 2–14) under the optimized geometries above. Based on the B3LYP/cc-pVTZ results, we performed the corresponding fitting curve in Fig. 3 and yielded the following equation:

$$\log Be\ (\mathrm{MHz}) = 5.0758 - 0.6370n + 0.0672n^2 - 4.04\times10^{-3}n^3 + 9.64\times10^{-5}n^4 \quad (2)$$

where n = 2–14. The fitting error and correlation coefficient are 0.00517 and 0.99996, respectively, exhibiting high accuracy. The rotational constants gradually decrease from 11.0821 GHz of HC_2N^+ to 0.0885 GHz of $HC_{14}N^+$ with an increase in the size of carbon chains. Obviously, the calculated rotational constants for HC_5N^+

Table 2
The calculated rotational constants (Be, GHz) and dipole moments (μ, Debye) of HC_nN^+ (n = 2–14) cations at the B3LYP/cc-pVTZ and CAM-B3LYP/cc-pVTZ levels.

Species	Be			μ	
	B3LYP	CAM-B3LYP	Expt.	B3LYP	CAM-B3LYP
HC_2N^+	11.0821	11.1760		4.3478	4.4704
HC_3N^+	4.5651	4.5940		4.9481	5.0904
HC_4N^+	2.3272	2.3394		5.7474	5.9536
HC_5N^+	1.3467	1.3530	1.3385[a]	6.2685	6.5263
HC_6N^+	0.8512	0.8549		6.8807	7.1457
HC_7N^+	0.5716	0.5739	0.5690[b]	7.3613	7.6939
HC_8N^+	0.4032	0.4048		7.8795	8.1964
HC_9N^+	0.2946	0.2957		8.3292	8.7462
$HC_{10}N^+$	0.2222	0.2230		8.7947	9.2003
$HC_{11}N^+$	0.1715	0.1720		9.2214	9.7351
$HC_{12}N^+$	0.1353	0.1358		9.6858	10.1500
$HC_{13}N^+$	0.1085	0.1088		10.0606	10.6983
$HC_{14}N^+$	0.0885	0.0888		10.4931	11.1418

[a] Experimental value from Ref. [17].
[b] Experimental value from Ref. [19].

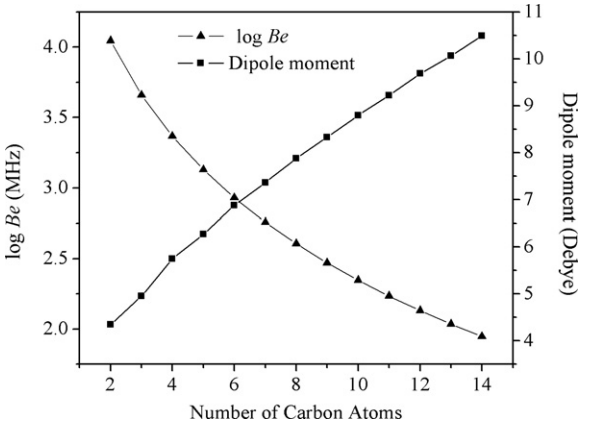

Fig. 3. The calculated rotational constants and dipole moments versus the number of carbon atoms n of HC_nN^+ (n = 2–14) cations optimized at the B3LYP/cc-pVTZ level.

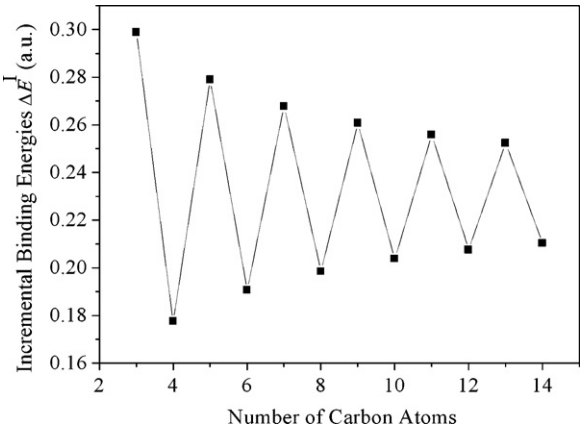

Fig. 5. Incremental binding energies ΔE^I (in atomic unit) of the linear ground-state HC_nN^+ clusters.

and HC_7N^+ agree reasonably with the corresponding experimental values (1.3385 GHz, 0.5690 GHz) [17,19], suggesting that the B3LYP/cc-pVTZ level is reliable. Approximate rotational constants are predicted by CAM-B3LYP/cc-pVTZ (see Table 2).

3.1.5. Dipole moments

As displayed in Table 2, the dipole moments of HC_nN^+ (n = 2–14) optimized by B3LYP/cc-pVTZ and CAM-B3LYP/cc-pVTZ levels are close to each other. It's clear to us from Fig. 3 that the dipole moments increase monotonically with an increase in the number of carbon atoms, which implies that the microwave spectra for longer carbon clusters tend to be collected more easily.

3.2. Energy differences (ΔE_n) and incremental binding energies (ΔE^I)

The relative stability of odd- and even-n HC_nN^+ analogues could be assessed by energy differences (ΔE_n) and incremental binding energies (ΔE^I) (see Table S2 in Supplementary Information). The energy difference is calculated as

$$\Delta E_n = E(HC_nN^+) - E(HC_{n-1}N^+) \quad (3)$$

where ΔE_n denotes the energy difference between a cluster and its previous neighboring cluster. The smaller the ΔE_n-value, the more stable is the cluster. Depicted in Fig. 4 are energy differences versus the number of carbon atoms (n). Apparently, the ΔE_n-values vary in a pattern of odd/even alternation: when n is odd, the ΔE_n-values are smaller than values of neighboring even-numbered clusters,

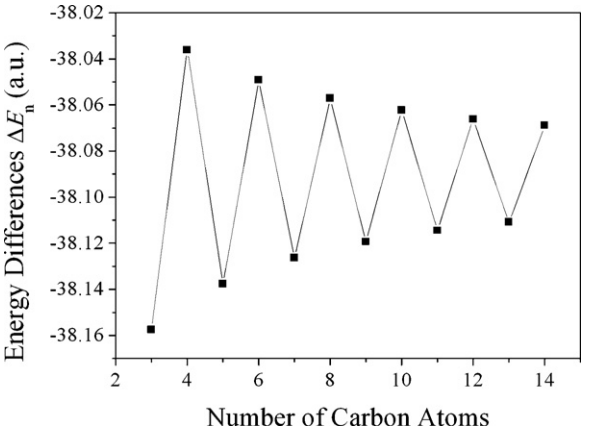

Fig. 4. Energy differences ΔE_n (in atomic unit) of the linear ground-state HC_nN^+ clusters.

making it clear that odd-n HC_nN^+ clusters are more stable than even-n counterparts.

The incremental binding energy (ΔE^I), another important parameter to estimate the relative stability of the investigated clusters [38], is predicted as the atomization energy (ΔE_a) difference of adjacent clusters. A larger ΔE^I implies a more stable cluster. It can be expressed as

$$\Delta E^I = \Delta E_a(HC_nN^+) - \Delta E_a(HC_{n-1}N^+) \quad (4)$$

where ΔE_a [39] denotes the energy difference between a molecule and its component atoms, i.e.,

$$\Delta E_a = [n \times E(C) + E(N) + E(H)] - E(HC_nN^+) \quad (5)$$

Fig. 5 displays the ΔE^I-values of HC_nN^+ (n = 2–14) clusters versus n. As expected, the values fluctuate following a contrary pattern of odd/even alternation to ΔE_n: when n is odd, the ΔE^I-values are larger compared to even-n isomers. From the result, we can further deduce that clusters with odd n are more stable than those with even n.

3.3. Vertical excitation energies

The ground state of the linear clusters HC_nN^+ (n = 2–14) is $X^2\Pi$ arising from the electronic configuration as follows:

$$(\text{Core})\,1\sigma^2 \ldots 1\pi^4 \ldots (n+2)\sigma^2 \ldots \left(\frac{n}{2}\right)\pi^4\left(\frac{n}{2}+1\right)\pi^1$$

× when n is even

$$(\text{Core})\,1\sigma^2 \ldots 1\pi^4 \ldots (n+2)\sigma^2 \ldots \left(\frac{n-1}{2}\right)\pi^4\left(\frac{n+1}{2}\right)\pi^3$$

× when n is odd

in which, the valance orbitals are comprised of $(2n+4)\sigma$ and $(2n+1)\pi$ electrons. Detailed valance electron configuration of ground-state HC_nN^+ (n = 2–14) is provided in Table S3 in Supplementary Information.

3.3.1. $HC_{2n}N^+$ (n = 3–7)

The vertical excitation energies (ΔE) and oscillator strengths (f) for the dipole-allowed $(2, 3)^2\Pi \leftarrow X^2\Pi$ and dipole-forbidden $1^2\Phi \leftarrow X^2\Pi$ transitions of $HC_{2n}N^+$ (n = 3–7) obtained by the CASPT2/cc-pVTZ level are summarized in Table 3, together with the available experimental data listed in parentheses.

Among the three selected electronic excitations, $2^2\Pi$ state is the lowest with the electronic transition from highest occupied

Table 3
The vertical excitation energies (ΔE, eV) and oscillator strengths (f) of selected three transitions for $HC_{2n}N^+$ (n = 3–7) using CASSCF active spaces in Table 1.

Species	State	Excitation	ΔE	f
HC_6N^+	$X^2\Pi$	$\ldots1\pi^4 2\pi^4 15\sigma^2 3\pi^4 4\pi^1 5\pi^0$	0.00	
	$2^2\Pi$	$3\pi \rightarrow 4\pi$	2.33 (2.17)[a](2.18)[c]	6.62×10^{-5}
	$1^2\Phi$	$3\pi \rightarrow 4\pi$	2.66	0.00
	$3^2\Pi$	$3\pi \rightarrow 4\pi$	3.01	2.15×10^{-5}
HC_8N^+	$X^2\Pi$	$\ldots2\pi^4 19\sigma^2 3\pi^4 4\pi^4 5\pi^1 6\pi^0$	0.00	
	$2^2\Pi$	$4\pi \rightarrow 5\pi$	2.02 (1.89)[a,b,c]	2.05×10^{-5}
	$1^2\Phi$	$4\pi \rightarrow 5\pi$	2.32	0.00
	$3^2\Pi$	$4\pi \rightarrow 5\pi$	2.57	1.98×10^{-5}
$HC_{10}N^+$	$X^2\Pi$	$\ldots3\pi^4 23\sigma^2 4\pi^4 5\pi^4 6\pi^1 7\pi^0$	0.00	
	$2^2\Pi$	$5\pi \rightarrow 6\pi$	1.76 (1.66)[a,b,c]	1.26×10^{-3}
	$1^2\Phi$	$5\pi \rightarrow 6\pi$	2.06	0.00
	$3^2\Pi$	$5\pi \rightarrow 6\pi$	2.25	7.64×10^{-7}
$HC_{12}N^+$	$X^2\Pi$	$\ldots27\sigma^2 4\pi^4 5\pi^4 6\pi^4 7\pi^1 8\pi^0$	0.00	
	$2^2\Pi$	$6\pi \rightarrow 7\pi$	1.58 (1.49)[a,b,c]	2.65×10^{-3}
	$1^2\Phi$	$6\pi \rightarrow 7\pi$	1.84	0.00
	$3^2\Pi$	$6\pi \rightarrow 7\pi$	2.02	3.02×10^{-4}
$HC_{14}N^+$	$X^2\Pi$	$\ldots31\sigma^2 5\pi^4 6\pi^4 7\pi^4 8\pi^1 9\pi^0$	0.00	
	$2^2\Pi$	$7\pi \rightarrow 8\pi$	1.44	4.49×10^{-3}
	$1^2\Phi$	$7\pi \rightarrow 8\pi$	1.66	0.00
	$3^2\Pi$	$7\pi \rightarrow 8\pi$	1.84	1.49×10^{-3}

[a] Experimental values from Ref. [20].
[b] Experimental values from Ref. [22].
[c] Experimental values from Ref. [23].

molecular orbital (HOMO) to single occupied molecular orbital (SOMO), that is, $n\pi \rightarrow (n+1)\pi$ in $HC_{2n}N^+$ clusters. The available experimental data (2.17, 1.89, 1.66, and 1.49 eV) [20,22] for $HC_{2n}N^+$ (n = 3–6) are well reproduced by the CASPT2 calculation, in which $2^2\Pi \leftarrow X^2\Pi$ transitions occur at 2.33, 2.02, 1.76, and 1.58 eV, respectively, with corresponding oscillator strengths (f) of 6.62×10^{-5}, 2.05×10^{-5}, 1.26×10^{-3}, and 2.65×10^{-3}. With the increase of n, $2^2\Pi \leftarrow X^2\Pi$ transitions of $HC_{2n}N^+$ clusters exhibit an f-increment trend, suggesting that electronic transitions are liable to be detected experimentally as the chain size increases. The next two excited states, $1^2\Phi$ and $3^2\Pi$, possess the same electronic transition as $2^2\Pi$ state. In accordance with the rules of spin and dipole, $1^2\Phi \leftarrow X^2\Pi$ transitions are dipole-forbidden and the related excitation energies are 2.66, 2.32, 2.06, 1.84, and 1.66 eV. The $3^2\Pi \leftarrow X^2\Pi$ transitions take place at 3.01, 2.57, 2.25, 2.02, and 1.84 eV, with corresponding oscillator strengths (f) of 2.15×10^{-5}, 1.98×10^{-5}, 7.64×10^{-7}, 3.02×10^{-4}, and 1.49×10^{-3}, respectively.

3.3.2. $HC_{2n+1}N^+$ (n = 2–6)

Table 4 presents the CASPT2 calculated vertical excitation energies (ΔE) and oscillator strengths (f) for the dipole-allowed $(2, 3)^2\Pi \leftarrow X^2\Pi$ and dipole-forbidden $1^2\Phi \leftarrow X^2\Pi$ transitions of $HC_{2n+1}N^+$ (n = 2–6). The available experimental data are also listed in parentheses.

As Table 4 shows, the strongest $2^2\Pi \leftarrow X^2\Pi$ transitions, arising from $n\pi \rightarrow (n+1)\pi$ excitation, are calculated to be 2.27, 2.04, 1.84, 1.62, and 1.49 eV, respectively, above the ground state and agree reasonably with experimental data (2.12, 1.84, 1.61, 1.42,

Table 4
The vertical excitation energies (ΔE, eV) and oscillator strengths (f) of selected three transitions for $HC_{2n+1}N^+$ (n = 2–6) using CASSCF active spaces in Table 1.

Species	State	Excitation	ΔE	f
HC_5N^+	$X^2\Pi$	$\ldots1\pi^4 13\sigma^2 2\pi^4 3\pi^3 4\pi^0$	0.00	
	$2^2\Pi$	$2\pi \rightarrow 3\pi$	2.27 (2.12)[a,b,c]	4.53×10^{-2}
	$3^2\Pi$	$3\pi \rightarrow 4\pi$	2.32	1.07×10^{-2}
	$1^2\Phi$	$3\pi \rightarrow 4\pi$	3.83	0.00
HC_7N^+	$X^2\Pi$	$\ldots2\pi^4 17\sigma^2 3\pi^4 4\pi^3 5\pi^0$	0.00	
	$2^2\Pi$	$3\pi \rightarrow 4\pi$	2.04 (1.85)[a](1.84)[b,c]	9.01×10^{-2}
	$3^2\Pi$	$4\pi \rightarrow 5\pi$	2.68	8.20×10^{-3}
	$1^2\Phi$	$4\pi \rightarrow 5\pi$	3.09	0.00
HC_9N^+	$X^2\Pi$	$\ldots21\sigma^2 3\pi^4 4\pi^4 5\pi^3 6\pi^0$	0.00	
	$2^2\Pi$	$4\pi \rightarrow 5\pi$	1.84 (1.61)[a,b,c]	1.56×10^{-1}
	$3^2\Pi$	$5\pi \rightarrow 6\pi$	2.23	1.50×10^{-2}
	$1^2\Phi$	$5\pi \rightarrow 6\pi$	2.53	0.00
$HC_{11}N^+$	$X^2\Pi$	$\ldots25\sigma^2 4\pi^4 5\pi^4 6\pi^3 7\pi^0$	0.00	
	$2^2\Pi$	$5\pi \rightarrow 6\pi$	1.62 (1.42)[a,b,c]	2.04×10^{-1}
	$3^2\Pi$	$6\pi \rightarrow 7\pi$	1.98	2.01×10^{-2}
	$1^2\Phi$	$6\pi \rightarrow 7\pi$	2.24	0.00
$HC_{13}N^+$	$X^2\Pi$	$\ldots4\pi^4 5\pi^4 6\pi^4 7\pi^3 8\pi^0$	0.00	
	$2^2\Pi$	$6\pi \rightarrow 7\pi$	1.49 (1.27)[a,b,c]	2.51×10^{-1}
	$3^2\Pi$	$7\pi \rightarrow 8\pi$	1.81	2.21×10^{-2}
	$1^2\Phi$	$7\pi \rightarrow 8\pi$	2.07	0.00

[a] Experimental values from Ref. [20].
[b] Experimental values from Ref. [22].
[c] Experimental values from Ref. [23].

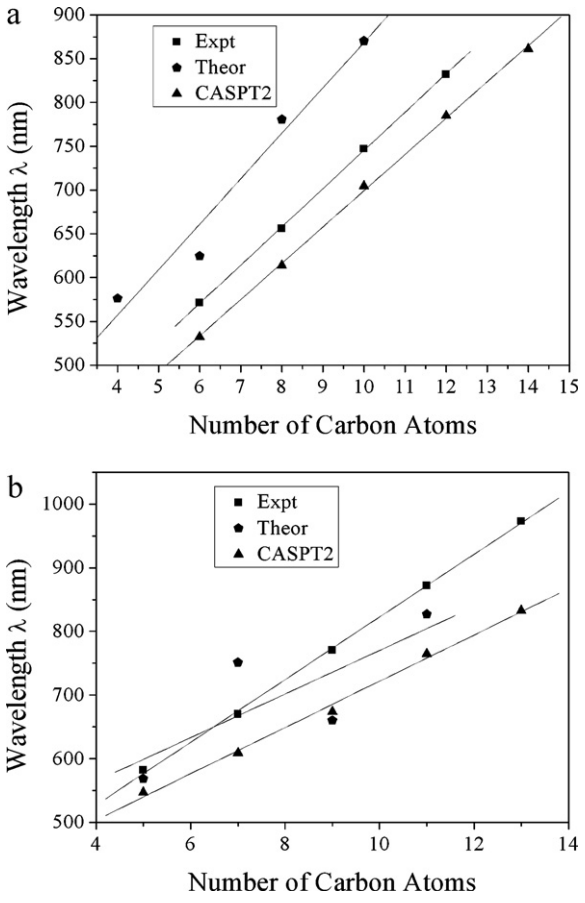

Fig. 6. The linear size dependence of the absorption wavelengths of the $2^2\Pi \leftarrow X^2\Pi$ transitions for $HC_{2n}N^+$ (n = 3–7) (a) and $HC_{2n+1}N^+$ (n = 2–6) (b) clusters by experiments, theories and CASPT2 calculations.

and 1.27 eV) [22,23]. The corresponding oscillator strengths (f) are 4.53×10^{-2}, 9.01×10^{-2}, 1.56×10^{-1}, 2.04×10^{-1}, and 2.51×10^{-1}. Apparently, the oscillator strengths increase gradually with the extension of carbon chains, which indicates that electronic transitions for longer chains should be observable more easily in further experiments. The $(n+1)\pi \rightarrow (n+2)\pi$ electron excitation gives rise to higher states $1^2\Phi$ and $3^2\Pi$. Excitation energies of $3^2\Pi$ excited state locate at 3.47, 2.68, 2.23, 1.98, and 1.81 eV, with corresponding oscillator strengths (f) of 6.51×10^{-3}, 8.20×10^{-3}, 1.50×10^{-2}, 2.01×10^{-2}, and 2.21×10^{-2}, respectively. The predicted dipole-forbidden $1^2\Phi$ states for $HC_{2n+1}N^+$ (n = 2–6) are higher in energy than the ground state by 3.83, 3.09, 2.53, 2.24, and 2.07 eV, respectively. According, the $3^2\Pi \leftarrow X^2\Pi$ transitions can be also observable experimentally for large oscillator strengths.

3.4. Size dependence of absorption wavelengths

As observed in the experimental studies, the absorption wavelengths of the origin bands for $2^2\Pi \leftarrow X^2\Pi$ transitions show remarkably linear size dependence upon the number of carbon atoms. Accordingly, we performed the linear fittings (see Fig. 6) based on data in Tables 3 and 4, and previous theoretical data [24]. For better comparison, linear fitting curves of $3^2\Pi \leftarrow X^2\Pi$ transitions were plotted in Fig. 7. We obtained the following equation:

$$\lambda = A + Bn \quad (6)$$

where n = 5–14, using the formula: λ [nm] = 1239.824 [nm × eV]/ΔE [eV].

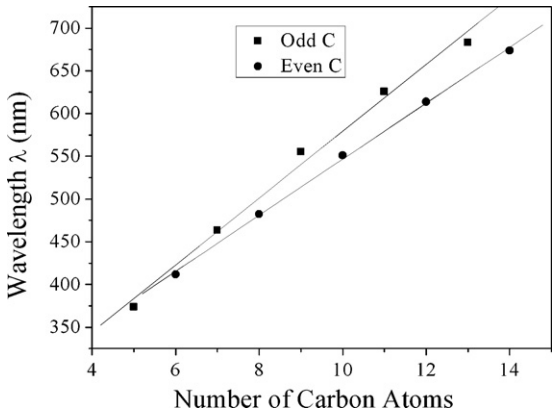

Fig. 7. The linear fitting curves for the $3^2\Pi \leftarrow X^2\Pi$ transitions of $HC_{2n}N^+$ (n = 3–7) and $HC_{2n+1}N^+$ (n = 2–6) by the CASPT2 calculations.

3.4.1. $HC_{2n}N^+$ (n = 3–7)

In the case of the experimental data in Fig. 6(a), A = 308.67 and B = 43.66. The fitting error and correlation coefficient are 1.90 nm and 0.9999, respectively, displaying high accuracy. In our equation predicted by CASPT2, A equals 284.87 and B equals 41.43 with fitting error and correlation coefficient 4.41 nm and 0.9996, respectively. Obviously, the two curves in Fig. 6(a) are close to each other very much and the obtained linear relationship can well reproduce the agreement of experimental and calculated data. However, we find no distinctive linear relationship in the previous data and the result may be in poor agreement with the experimental findings.

For $3^2\Pi \leftarrow X^2\Pi$ transitions, as shown in Fig. 7, we find that linear size dependence for the absorption wavelength of even-n clusters is more prominent compared to odd-n counterparts, with corresponding fitting error of 4.17 nm, 13.63 nm and correlation coefficient of 0.9994, 0.9955, respectively.

3.4.2. $HC_{2n+1}N^+$ (n = 2–6)

It can be seen from Fig. 6(b) that in terms of the experimental data, A = 335.85 and B = 48.75, whose accuracy is also very high with corresponding fitting error and correlation coefficient 4.27 nm and 0.9997, respectively. For our CASPT2 calculated results, A = 358.24 and B = 36.35 with fitting error and correlation coefficient 9.11 nm and 0.9977, respectively. Likewise, the linear relationship for the previous data is less pronounced than for our calculations as shown in Fig. 6(b).

3.5. Dissociation channels

The possible dissociation channels of HC_nN^+ clusters are complicated. Nevertheless we do not intend to characterize the reaction pathways and transition states for fragmentation but to evaluate the relative stability of the clusters in terms of fragmentation energies based on hypothetical reactions. The six dissociation channels predicted in the paper are presented as follows:

$$HC_nN^+ \rightarrow HC_{n-1}N^+ + C \quad (R1)$$

$$HC_nN^+ \rightarrow HC_{n-2}N^+ + C_2 \quad (R2)$$

$$HC_nN^+ \rightarrow HC_{n-3}N^+ + C_3 \quad (R3)$$

$$HC_nN^+ \rightarrow HC_n^+ + N \quad (R4)$$

$$HC_nN^+ \rightarrow C_n^+ + HN \quad (R5)$$

$$HC_nN^+ \rightarrow C_nN^+ + H \quad (R6)$$

Fig. 8 shows fragmentation energies related to different dissociation channels versus n. As displayed in Fig. 8, we can find a distinct odd/even alternation that the fragmentation energies of

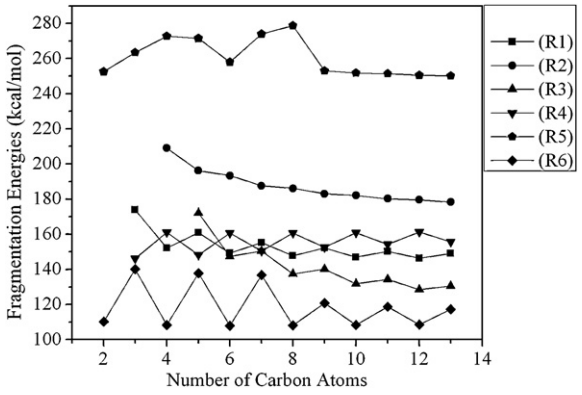

Fig. 8. Fragmentation energies (in atomic unit) versus the number of carbon atoms *n*.

odd-*n* HC_nN^+ are always larger than values of even-*n* HC_nN^+ for reactions (R1) and (R3). The results are consistent with the previous conclusion in this paper that HC_nN^+ clusters with odd *n* are relatively more stable. The ejection of odd-numbered carbon atoms will lead to an inverse in parity of the clusters and the more stable odd-*n* clusters require more energy for dissociation than the less stable even-*n* ones. However, the loss of a C_2 fragment in reaction (R2) does not cause change in parity of the parent cationic clusters and the odd/even alternation effect is less apparent than that of reactions (R1) and (R3). Meanwhile, the fragmentation energies are higher for the loss of C_2 than for the loss of C or C_3. The phenomenon is in accordance with report on fragmentation energies of C_n^- in previous literature [40]. The dissociation energy of the loss of H in reaction (R6), showing similar odd/even alternation with reactions (R1) and (R3), exhibits quite distinct parity rule from that of the loss of N in reaction (R4). Compared with reaction (R4) in relation to the breaking of a C–N bond, reaction (R5) needs more energy because there exists the break of a C–N as well as a C–H bond. Reaction (R6), involving the ejection of a H fragment, needs the lowest energy and is likely to be the dominant dissociation pathway.

4. Conclusions

The ground-state structures of linear HC_nN^+ (n = 2–14) clusters are stable according to frequency analyses. The present work indicates that odd-numbered clusters possess polyacetylene-like structures, i.e., a series of alternate single–triple bonds along the C_n chains, whereas there is a cumulenic character in even-*n* series. The regularity that odd-*n* cationic clusters are more stable than the even-*n* analogues has been illustrated according to studies on the properties of ground-state bonding characters, energy differences (ΔE_n), and incremental binding energies (ΔE^1).

On the other hand, the CASPT2 calculated vertical excitation energies for $2^2\Pi \leftarrow X^2\Pi$ of HC_nN^+ (n = 5–13) transitions are 2.27, 2.33, 2.04, 2.02, 1.84, 1.76, 1.62, 1.58, and 1.49 eV, respectively, matching very well with observed bands at 2.12, 2.17, 1.84, 1.89, 1.61, 1.66, 1.42, 1.49, and 1.27 eV. The corresponding absorption wavelengths present remarkable linear size dependence as shown in experimental observations. The oscillator strengths of dipole-allowed transitions increase with the extension of carbon chains, which suggests that electronic spectra of longer carbon chains are detectable more easily from an experimental point of view. In addition, we investigated the higher excited electronic transitions for HC_nN^+ (n = 5–14) clusters, which should be responsible for assignments of the experimental bands. To sum up, calculations in this article may provide accurate information for spectroscopist and contribute to further experimental research.

Acknowledgments

The authors thank the State Key Laboratory of Physical Chemistry of Solid Surfaces for providing computational resources and the National Science Foundation of China (Grant No. 21003036) and Science Foundation of Henan University (Grant No. SBGJ090507) for financial supports.

Appendix A. Supplementary data

Supplementary data associated with this article can be found, in the online version, at doi:10.1016/j.ijms.2011.08.025.

References

[1] M.C. McCarthy, M.J. Travers, A. Kovacs, C.A. Gottlieb, P. Thaddeus, Astrophys. J. Suppl. Ser. 113 (1997) 105–120.
[2] T. Giesen, Molecular Astrophysics: The Search for Interstellar Carbon Clusters, 16–20 September, Han-sur-Lesse, Belgium, 2002.
[3] Th. Henning, F. Salama, Science 282 (1998) 2204–2210.
[4] J.M. Greenberg, C. Shen, Astrophys. Space Sci. 269–270 (1999) 33–55.
[5] P. Ehrenfreund, S.B. Charnley, Annu. Rev. Astron. Astrophys. 38 (2000) 427–483.
[6] A. Van Orden, R.J. Saykally, Chem. Rev. 98 (1998) 2313–2357.
[7] M.C. McCarthy, P. Thaddeus, J. Mol. Spectrosc. 232 (2005) 351–357.
[8] D.J. Peeso, D.W. Ewing, T.T. Curtis, Chem. Phys. Lett. 166 (1990) 307–310.
[9] A. Zaidi, S. Lahmar, Z.B. Lakhdar, P. Rosmus, M. Hochlaf, Theor. Chem. Acc. 114 (2005) 341–349.
[10] T.W. Schmidt, A.E. Boguslavskiy, T. Pino, H. Ding, J.P. Maier, Int. J. Mass Spectrom. 228 (2003) 647–654.
[11] F.J. Mazzotti, E. Achkasova, R. Chauhan, M. Tulej, P.P. Radi, J.P. Maier, Phys. Chem. Chem. Phys. 10 (2008) 136–141.
[12] J.H. Kiefer, S.S. Sidhu, R.D. Kern, K. Xie, H. Chen, L.B. Harding, Combust. Sci. Technol. 82 (1992) 101–130.
[13] H. Kroto, Int. J. Mass Spectrom. 200 (2000) 253–260.
[14] M.C. McCarthy, J.-U. Grabow, M.J. Travers, W. Chen, C.A. Gottlieb, P. Thaddeus, J. Astrophys. 494 (1998) 231–234.
[15] P. Thaddeus, M.C. McCarthy, M.J. Travers, C.A. Gottlieb, W. Chen, Faraday Discuss. 109 (1998) 121–135.
[16] M.B. Bell, P.A. Feldman, M.J. Travers, M.C. McCarthy, C.A. Gottlieb, P. Thaddeus, Astrophys. J. Lett. 483 (1997), L61 L64.
[17] W.E. Sinclair, D. Pfluger, J.P. Maier, J. Chem. Phys. 111 (1999) 9600–9608.
[18] A.M. Smith, A. Jürgen, V.E. Bondybey, Chem. Phys. Lett. 244 (1995) 379–387.
[19] W.E. Sinclair, D. Pfluger, D. Verdes, J.P. Maier, J. Chem. Phys. 112 (2000) 8899–8903.
[20] R. Nagarajan, J.P. Maier, Int. Rev. Phys. Chem. 29 (2010) 521–554.
[21] J. Fulara, S. Leutwyler, J.P. Maier, U. Spittel, J. Phys. Chem. 89 (1985) 3190–3193.
[22] J.P. Maier, Chem. Soc. Rev. 26 (1997) 21–28.
[23] D. Forney, P. Freivogel, J. Fulara, J.P. Maier, J. Chem. Phys. 102 (1995) 1510–1514.
[24] J.M. Lee, L. Adamowicz, Spectrochim. Acta Part A 57 (2001) 897–906.
[25] Z.X. Cao, S.D. Peyerimhoff, Phys. Chem. Chem. Phys. 3 (2001) 1403–1406.
[26] J.Y. Qi, M.D. Chen, W. Wu, Q.E. Zhang, C.T. Au, Chem. Phys. 364 (2009) 31–38.
[27] J.L. Zhang, X.G. Guo, Z.X. Cao, Int. J. Mass Spectrom. 290 (2010) 113–119.
[28] J.L. Zhang, X.G. Guo, Z.X. Cao, J. Chem. Phys. 131 (2009), 144307-1–144307-7.
[29] X.G. Guo, J.L. Zhang, J.F. Li, L.H. Jiang, J.L. Zhang, Chem. Phys. 360 (2009) 27–31.
[30] C. Lee, W. Yang, R.G. Parr, Phys. Rev. B 37 (1988) 785–789.
[31] P.J. Stephens, F.J. Devlin, C.F. Chabalowski, M.J. Frich, J. Phys. Chem. 98 (1994) 11623–11627.
[32] A.D. Becke, J. Chem. Phys. 98 (1993) 5648–5652.
[33] T. Yanai, D.P. Tew, N.C. Handy, Chem. Phys. Lett. 393 (2004) 51–57.
[34] P.J. Celani, H.-J. Werner, J. Chem. Phys. 112 (2000) 5546–5557.
[35] S.D. Peyerimhoff, in: P. von R. Schleyer, N.L. Allinger, T. Clark, J. Gasteiger, P.A. Kollman, H.F. Schaefer, P.R. Schreiner (Eds.), The Encyclopedia of Computational Chemistry, vol. 4, Wiley, Chichester, 1998, p. 2654.
[36] M.J. Frisch, G.W. Trucks, H.B. Schlegel, G.E. Scuseria, M.A. Robb, J.R. Cheeseman, G. Scalmani, V. Barone, B. Mennucci, G.A. Petersson, H. Nakatsuji, M. Caricato, X. Li, H.P. Hratchian, A.F. Izmaylov, J. Bloino, G. Zheng, J.L. Sonnenberg, M. Hada, M. Ehara, K. Toyota, R. Fukuda, J. Hasegawa, M. Ishida, T. Nakajima, Y. Honda, O. Kitao, H. Nakai, T. Vreven, J.A. Montgomery Jr., J.E. Peralta, F. Ogliaro, M. Bearpark, J.J. Heyd, E. Brothers, K.N. Kudin, V.N. Staroverov, R. Kobayashi, J. Normand, K. Raghavachari, A. Rendell, J.C. Burant, S.S. Iyengar, J. Tomasi, M. Cossi, N. Rega, J.M. Millam, M. Klene, J.E. Knox, J.B. Cross, V. Bakken, C. Adamo, J. Jaramillo, R. Gomperts, R.E. Stratmann, O. Yazyev, A.J. Austin, R. Cammi, C. Pomelli, J.W. Ochterski, R.L. Martin, K. Morokuma, V.G. Zakrzewski, G.A. Voth, P. Salvador, J.J. Dannenberg, S. Dapprich, A.D. Daniels, O. Farkas, J.B. Foresman, J.V. Ortiz, J. Cioslowski, D.J. Fox, Gaussian 09, Revision A.02, Gaussian, Inc., Wallingford CT, 2009.
[37] MOLPRO 2006.1, a package of *ab initio* programs, H.-J. Werner, P.J. Knowles, R. Lindh, F.R. Manby, M. Schütz, and others.
[38] G. Pascoli, H. Lavendy, Int. J. Mass Spectrom. Ion Process. 173 (1998) 41–54.
[39] J.B. Foresman, A. Frisch, Exploring Chemistry with Electronic Structure Methods, Gaussian, Inc., Pittsburgh, PA, 1996.
[40] F. Lépine, A.R. Allouche, B. Baguenard, Ch. Bordas, M. Aubert-Frécon, J. Phys. Chem. A 106 (2002) 7177–7183.